Auburn University

Department of Civil and Environmental Engineering

Technical Report

Investigation of air-water interactions in the Interconnector Sewer in Columbus, OH

Jose G. Vasconcelos, Ph.D.

Robson L. Pachaly, M.S

Final Version

June, 2021

Contents

1 Motivation and Background **7**

2 Report Structure **8**

3 Part 1: 1D analysis of system flows using HAST **9**

3.1 Methodology 9

3.1.1 Geometry conditions 9

3.1.2 Inflows and outflows conditions 10

3.1.3 Ventilation conditions 11

3.2 Simulation scenarios and results 12

3.2.1 Scenario 1: Simulation of conditions in MH1 for the 3/20/20 inflows 12

3.2.2 Alternative scenario: Effects of twin-barreled INT 16

4 Part 2: 3D analysis of system flows using OpenFOAM **18**

4.1 Methodology 18

4.1.1 System Geometry 18

4.1.2 Mesh Generation 20

4.1.3 OpenFOAM Solver 22

4.1.4 Initial Conditions 24

4.1.5 Boundary Conditions 25

4.1.6 Cluster & parallelization 26

4.2 Simulation results and discussion 26

4.2.1 Scenario 1: Complete Pump Failure 27

4.2.2 Scenario 2: Pump failure to a flow rate of 110 MGD 30

4.2.3 Scenario 3: Pump failure to a flow rate of 219 MGD 33

4.2.4 Scenario 4: Pump Failure 329 MGD 36

4.2.5 Summary of all CFD Simulation 39

5 Part 3: Alternative INT design with ventilated MH1 **42**

5.1 Simulation conditions 42

5.2 Simulation results 42

6 Final remarks **45**

List of Figures

1 Location of MH1 with respect to IJC and nearby sewer lines, and damage following 3/25 flow interruption 8
2 Inflows and outflow hydrographs from INT, BWO, BWARI and IJC used in the representation of the unsteady flow conditions in March 20, 2020. The start time of the hydrographs is at 12:00 AM, 3/20/20 10
3 Geometric characteristics of MH1, indicating a concrete cap with volume of 140 ft^3 and no ventilation. 13
4 Geometric characteristics of MH1, indicating a concrete cap with volume of 140 ft^3 and no ventilation. 13
5 Comparison between SCADA measurements (5-minute interval) of IJC water level and the predictions by HAST model. 14
6 Computation of air-phase pressure forces acting on MH1. The threshold for the displacement of the top concrete structure in MH1 is 7.3 tons. 15
7 Comparison of air phase pressures at MH1 between the singe barrel solution (Blue) when a second sewer line is installed at the terminal reaches in INT (Orange). There is a predicted decrease in the peak surge, but air phase pressure still exceeds the threshold for the motion of the top concrete structure in MH1 of 7.3 tons. 16
8 Important elements represented by the CFD geometry 19
9 Mesh at IJC 21
10 Computational cells on pipes and chambers cross-sections. Not shown to scale. 21
11 Finer mesh at IJC 22
12 compressibleInterFoam Steady State 27
13 Scenario 1: Maximum peak level 28

14 Scenario 1: Pressure head variation at IJC for CFD scenario 1 along with HAST results 29
15 Scenario 1: Pressure head variation at MH1 for CFD Scenario 1. 30
16 Scenario 2: Maximum peak level 31
17 Scenario 2: Pressure variation at IJC 32
18 Scenario 2: Pressure variation at MH1 for CFD scenario 2 33
19 Scenario 3: Maximum peak level 34
20 Scenario 3: Pressure head variation at IJC for CFD scenario 3 35
21 Scenario 3: Pressure head variation at MH1 for CFD scenario 3 36
22 Scenario 4: Maximum peak level 37
23 Scenario 4: Pressure head variation at IJC for CFD scenario 4 38
24 Scenario 4: Pressure head variation at MH1 for CFD scenario 4 39
25 CFD simulation results considering all scenarios for IJC 40
26 CFD simulation results considering all scenarios for MH1 41
27 Comparison of head elevation between IJC and MH1 for a scenario where there is a 12-in ventilation tower at MH1. 43

Abbreviations

BWARI Big Walnut Augmentation Rickenbacker Interceptor

BWO Big Walnut Outfall

CFD Computational Fluid Dynamics

HAST Hydraulic Analysis of Sewers and Tunnels

ISOC Interconnector Sewer Outlet Chamber

IJC Influent Junction Chamber

INT Interconnector Sewer

MGF Million Gallons a Day

MH1 Manhole 1

TPA Two-component Pressure Approach

VOF Volume-of-Fluid

WWTP Wastewater Treatment Plant

Nomenclature

α	Phase fraction
β	Turbulence-model constant
μ	Coefficient of viscosity
ν	Kinematic viscosity
ω	Specific dissipation of turbulence kinetic energy
ρ	Density
σ	Turbulence-model constant
C_p	Specific heat
f	Body forces
k	Thermal conductivity
p	Pressure
P_k	Production of turbulence kinetic energy
S_T	source terms in the energy equation
S_u	Source terms in the momentum equation
T	Temperature
t	Time
u	Fluid velocity

1 Motivation and Background

The Southerly Wastewater Treatment Plant (WWTP) is the largest treatment facility operated by the Northeast Ohio Regional Sewer District, serving more than 500 thousand residents in the Columbus, OH metropolitan area. The facility treats combined sewerage that arrives in the plant through a large hydraulic structure named *Influent Junction Chamber*, hereon referred to as *IJC*. The IJC receives inflows from three main sewer lines: Big Walnut Outfall (BWO), Big Walnut Augmentation Rickenbacker Interceptor (BWARI), and he Interconnector Sewer (INT). These inflows are transferred to the WWTP through several pumps that are activated according to the inflows arriving at IJC.

Following severe rain events in March 19 and 20, 2020 with subsequent large increase of inflows arriving at IJC, the pump station was operating at large inflows, in the range of 660 MGD (28.9 m^3/s). Shortly before noon on 3/20 there was a sudden and complete flow interruption in the pumps within IJC for near one minute, leading to an immediate increase on the IJC water levels. An inspection on the INT sewer following the event determined a structural damage in a non-ventilated manhole structure immediately upstream from IJC, referred hereon as *MH1*. The hypothesis is that this damage was triggered by the sudden flow changes at IJC caused by the pump flow stoppage and MH1 characteristics, which is verified through the investigation presented in this technical report.

This report aims to: 1) study the flow conditions in the IJC and nearby sewers; 2) to determine to what extent ventilation restrictions contributed toward the damage observed in MH1; and 3) to determine whether placing ventilation at MH1 can prevent air-related damage if flows are abruptly changed in the system.

FIG. 1. Location of MH1 with respect to IJC and nearby sewer lines, and damage following 3/25 flow interruption

2 Report Structure

This report is structured in three main parts:

- Part 1 will present the one-dimensional analysis of the events associated with the IJC pump flow interruption using the HAST model.
- Part 2 will present further insights on the rapid change in flow conditions following the IJC pump flow interruption using three-dimensional CFD model results.
- Part 3 will present design recommendations to avoid potential problems in INT due to the lack of ventilation in the structure.

3 Part 1: 1D analysis of system flows using HAST

3.1 Methodology

3.1.1 Geometry conditions

The development of the one-dimensional modeling of the unsteady flows in the INT, IJC and connected systems was performed with the use of the HAST model. The model solves the Saint-Venant equations adapted to represent pressurized flows with the Two-component Pressure Approach (Vasconcelos et al. 2006) and using a non-linear numerical scheme built within a finite-volume model. Further modifications in HAST enables it to account for air pocket entrapment, pressurization, and release through incorporating a set of ordinary differential equations in the regions that have entrapped air, as is explained in (Vasconcelos et al. 2015).

In terms of geometry of the system, the implementation of the sewers and structures followed the nomenclature and characteristics of a SWMM5 model that was provided by ARCADIS. These are the general characteristics of the sewers comprising the model:

- INT: Initially, the upstream end of the INT was set the junction "0107S0001", which is located approximately 35 thousand feet upstream from IJC. In order to improve the representation of the inflow time series routing from INT, later the upstream end of INT in the simulation was moved to junction "0589S0068", which is about 3 thousand feet upstream from IJC. Later in the development of the work, another change was implemented in which INT splits into two 104-in parallel sewer lines at the Sewer Outlet Chamber (SOC). This geometry change reflects the Second Barrel Interconnector Augmentation Project. The results that are presented in this report reflect the existence of this two parallel sewer lines.
- BWO: The upstream end of this system was at the junction "West WYE Structure", with the downstream end at IJC. The lengths considered in the simulation was about 30 thousand feet.

- BWARI: The upstream end of this system was at the junction "0261S0117", with the downstream end at IJC. The lengths considered in the simulation was about 35 thousand feet. There was also a spur sewer that connects to BWARI- the Lockbourne Intermodal Subtrunk - which was added to the model.

3.1.2 Inflows and outflows conditions

At each upstream end of the sewers connected to IJC (INT, BWO and BWARI) there are inflows that were included in the HAST model based on the results from SWMM model results provided by ARCADIS. There is a single outflow point at IJC, and the values adopted there were based on SCADA data, with 1-second resolution. The simulation start time is 9 hours prior to the failure of the pumps in IJC. In order to accelerate the warm-up time of the model, the IJC outflow in the initial 4.5 hours of the simulation was calibrated so that HAST results would better represent the IJC water level, which was also based on SCADA data.

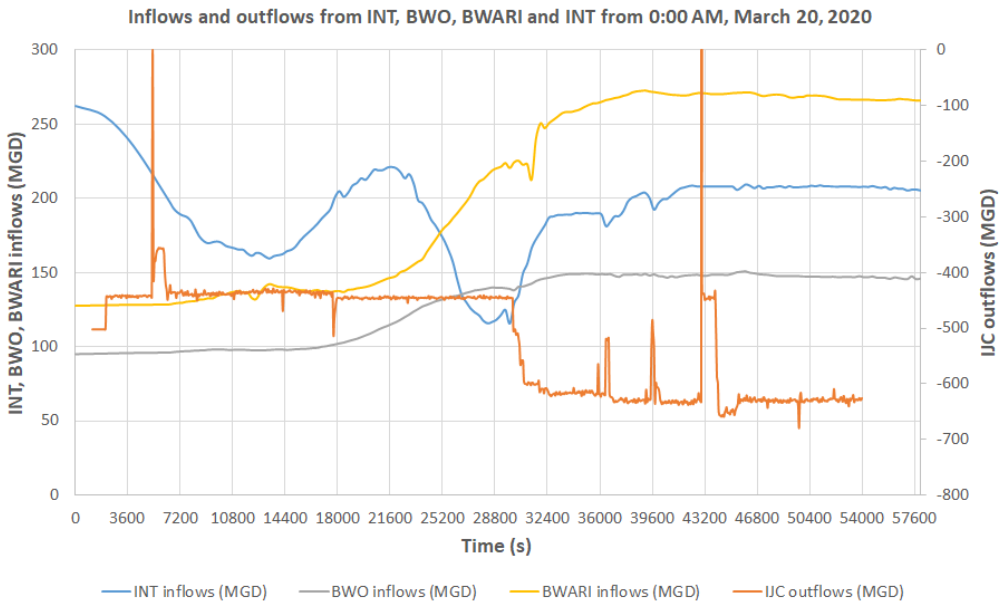

FIG. 2. Inflows and outflow hydrographs from INT, BWO, BWARI and IJC used in the representation of the unsteady flow conditions in March 20, 2020. The start time of the hydrographs is at 12:00 AM, 3/20/20

As Figure 2 indicates, there are significant inflow changes in 3/20/2020, particularly at INT sewer. At about 6:00 AM inflows from BWO and BWARI begin to ramp up and about 8:30 AM all pumps are operating in IJC with a resulting outflow in the range of 660 MGD. Except by some short-duration fluctuations at 10 AM and 11 AM, all pumps remain in operation. Then suddenly, a little before 12:00 PM the complete flow interruption at IJC pumps zeroes the outflow from the system for 57 seconds. Outflows are then re-established first in the range of 440 MGD, then with the full range of 660 MGD.

Within HAST, these inflows and outflows take place at structures that correspond to boundary conditions in the model. At each of these locations, flows are solved with the application of principles of mass conservation, energy equation and the characteristic equations. Within selected locations overflows were observed during the simulation, consistent with the elevation of the overflow point. Details of the mathematical implementation of HAST are outside of the scope of this report.

3.1.3 Ventilation conditions

Of particular interest are the assumptions with regards to the ventilation within the structures. The following was assumed with respect to ventilation in the model:

- It was assumed that a 4-ft diameter pipe provided ventilation for IJC, and this ventilation was placed at the top of the IJC structure
- Regarding the manholes at INT between SOC and IJC: Initial models were constructed with the assumption that these structures were not ventilated. Subsequently, it was assumed that MH1 was provided with a 1-ft ventilation pipe, with an opening to atmosphere at elevation 691 ft.
- All remaining structures in the model were assumed to have unhindered ventilation

3.2 Simulation scenarios and results

As it was pointed earlier, the numerical study of the flow conditions at INT took place in stages as geometry changes were implemented in the model. Results presented in the report correspond to the final geometric configuration, which considered: 1) A shorter INT geometry; 2) overflow elevation at IJC (physically placed near the downstream end of BWO) set at 684 ft due to flood stage in the River Scioto caused by the rain in March 19 and 20. This scenario is used to estimate the forces acting on MH1 during the pump failure in 3/20/20.

An additional scenario is added to this report, given that it is planned the installation of a parallel 104-in diameter sewer line linking the SOC to IJC. In this part, the simulations for this condition also assume that there is no ventilation in MH1.

3.2.1 Scenario 1: Simulation of conditions in MH1 for the 3/20/20 inflows

MH1 is the structure on INT immediately upstream from IJC, and currently it does not have any ventilation, as it is indicated in Figure 3. This structure has an estimated concrete volume of 124 ft^3, with a resulting weight of 18.6 KIPS or 9 tons-force.

The lack of ventilation on MH1 results in the entrapment of the overhead air in the structure whenever the hydraulic grade line in INT exceeds the sewer obvert. At this point, the air phase exceeds atmospheric pressure, with the additional characteristic of the compressibility and elasticity of air phase exceeding those of water. This is an important characteristic as this changes the force balance within the manhole headspace as water levels (W.L.) varied during the pump failure at IJC, as it is illustrated in Figure 4

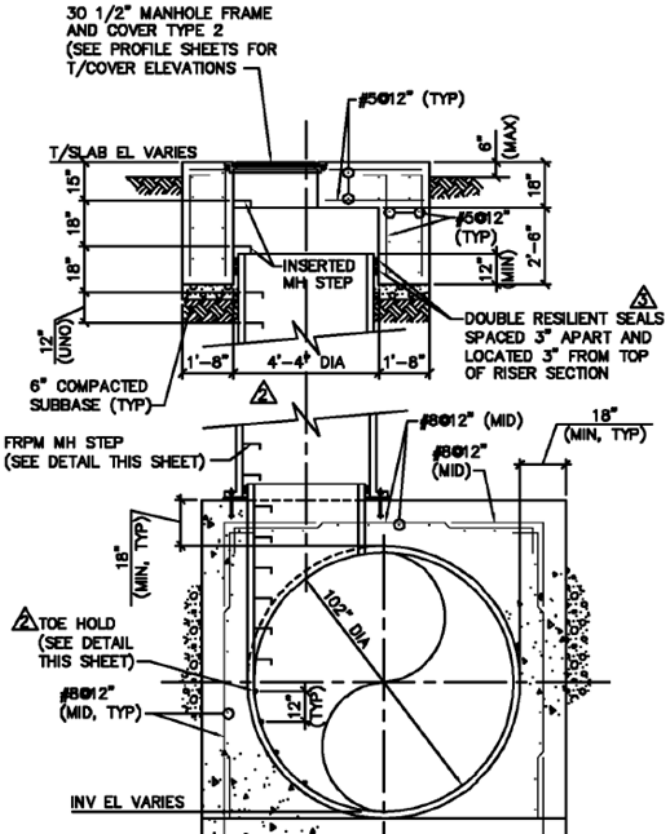

FIG. 3. Geometric characteristics of MH1, indicating a concrete cap with volume of 140 ft^3 and no ventilation.

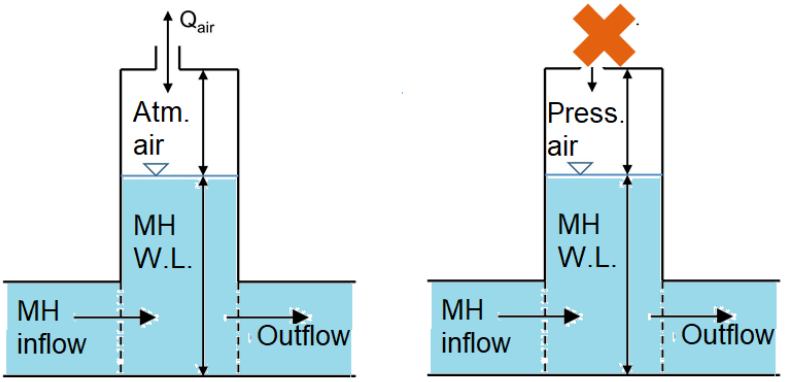

FIG. 4. Geometric characteristics of MH1, indicating a concrete cap with volume of 140 ft^3 and no ventilation.

Simulation results yielded by HAST indicate that the representation of IJC water level for March 20 is fairly accurate, given the uncertainties associated with the inflows that were admitted to the system during the day. These water level results, shown in Figure 5, were obtained using inflows provided by a SWMM model, and the outflows from the SCADA system for IJC pumps. With the adequate water level results, the calculation of the forces acting on MH1 was possible.

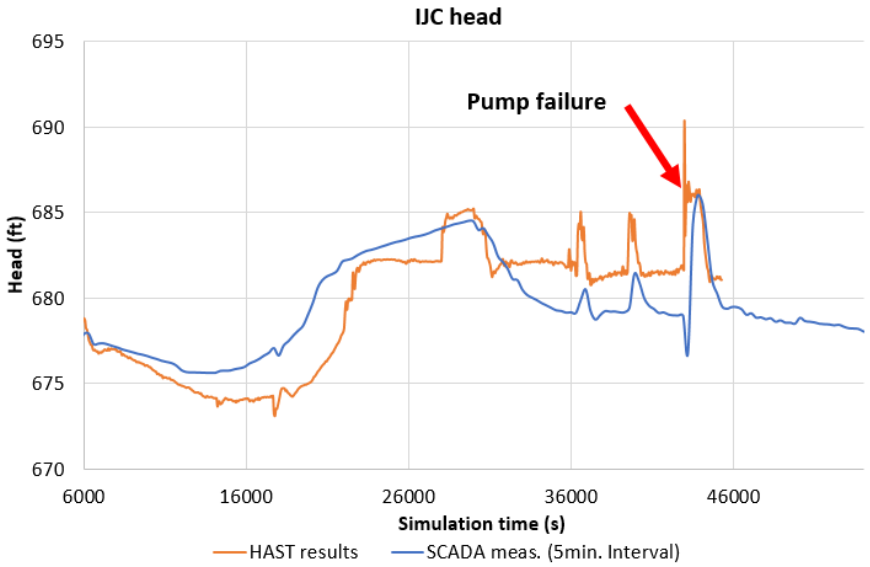

FIG. 5. Comparison between SCADA measurements (5-minute interval) of IJC water level and the predictions by HAST model.

During the event, when the MH1 failure occurred, the water level created by the river flood reached an elevation of 684 ft, thus covering the concrete cap that was at a grade elevation near 678.5 ft. In such conditions, there were five vertically-oriented forces acting on the concrete cap structure presented in Figure 3:

1. Concrete structure weight, 140 ft^3 of volume, weight of 9.9 ton-force, downward
2. Hydrostatic pressure force acting on the top of structure, 7'8" diameter, depth of 5.5 ft, 7.2 ton-force, downward

3. Hydrostatic pressure force acting on the 1'8" wide outer concrete ring with center line diameter of 6 ft, positioned 4 ft below the top slab, equal to 8.5 ton-force, upward.
4. Buoyancy force created by the air cavity underneath the concrete structure, volume of 50.5 ft^3, 1.4 ton-force, upward.
5. Dynamically varying air phase pressure force due to the lack of ventilation in MH1

Force components from 1 to 4 result in a downward resulting force of 7.1 ton-force. Thus, if the air phase pressure force would exceed this threshold it would be possible for the structure to be displaced. As it is indicated in Figure 6, HAST modeling results indicated that this threshold is exceeded during the pump failure, offering an explanation for the failure of MH1.

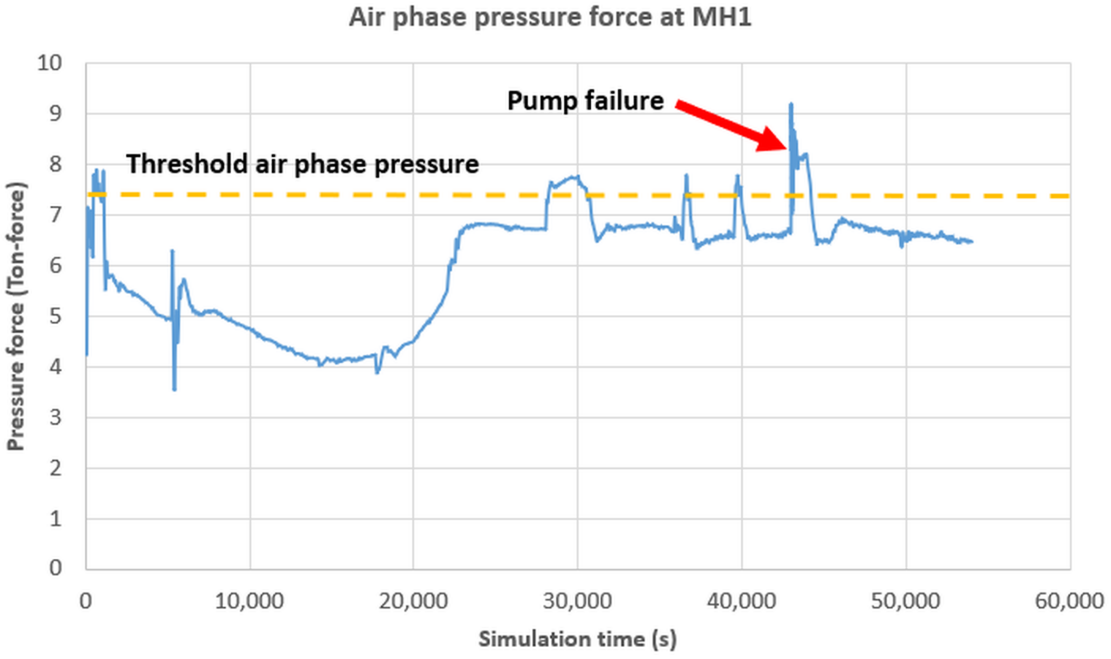

FIG. 6. Computation of air-phase pressure forces acting on MH1. The threshold for the displacement of the top concrete structure in MH1 is 7.3 tons.

3.2.2 Alternative scenario: Effects of twin-barreled INT

Two additional scenarios were considered in this report, and the first one presented here is the case when there is a second barrel linking the Sewer Outlet Chamber (SOC) near the downstream end of INT to IJC via a second parallel sewer with 104-in diameter. In this scenario, MH1 remains unventilated, and this scenario objective is to compare the difference in pressures results. The geometry of the INT sewer was adjusted in the model HAST, and simulation conditions were run.

The results, presented in Figure 7, indicate that there was a drop in the air pressure, but the threshold for the displacement of the concrete cap is still exceeded. A subsequent modification on the twin-barreled condition for INT is presented in Part 3 of this report, where the ventilation of MH1 is included.

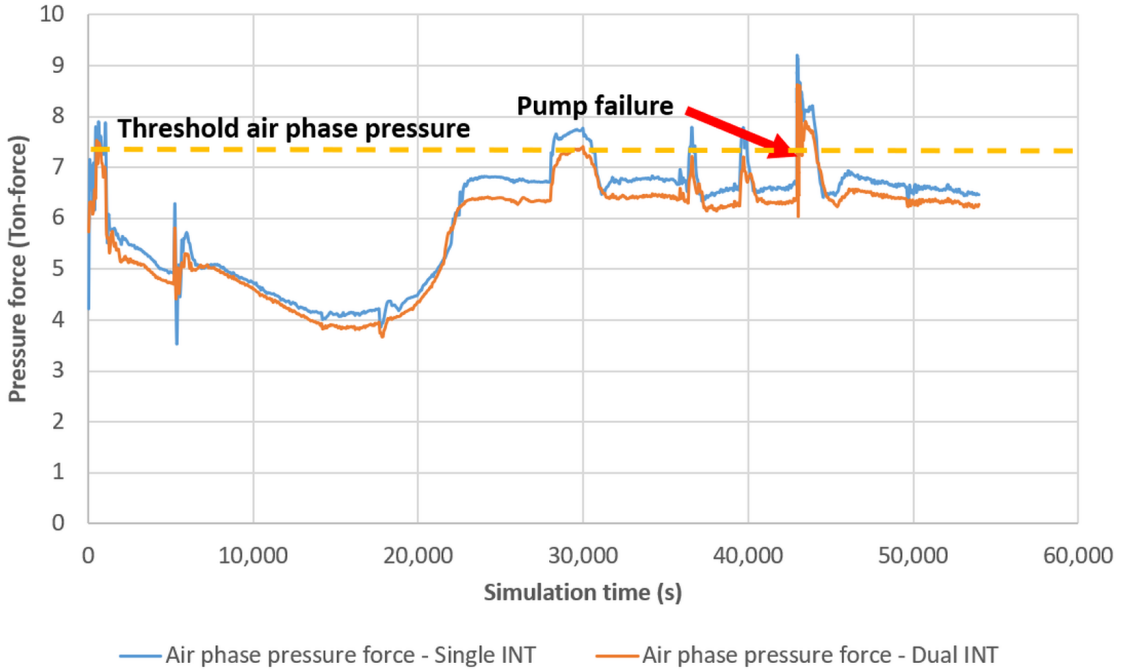

FIG. 7. Comparison of air phase pressures at MH1 between the singe barrel solution (Blue) when a second sewer line is installed at the terminal reaches in INT (Orange). There is a predicted decrease in the peak surge, but air phase pressure still exceeds the threshold for the motion of the top concrete structure in MH1 of 7.3 tons.

Based on these findings, an alternative solution where the MH1 top slab is ventilated was proposed. Simulation result using this alternative are presented in Part 3 of this report. In addition, a separate evaluation of air pressurization observed in the filling process of INT and nearby structures were studied with the CFD tool, as is presented in Part 2.

4 Part 2: 3D analysis of system flows using OpenFOAM

4.1 Methodology

The hydraulic behavior of the INT sewer, as well the terminal points of BWO and BWARI sewers were studied for two events that correspond to a partial a total failures of the pumps in the IJC chamber. This part of the report focuses on the characterization of the flow at IJC and INT using a Computational Fluid Mechanics (CFD) 3-D modeling approach. The 3-D simulation was performed using the OpenFOAM software (OpenCFD 2019), which is a well-established platform for computational fluid dynamics modeling. The results of both modeling efforts were compared for gaining insights of air-water interactions in this system when a situation of a pump failure during intense inflows/rainfalls occurs.

4.1.1 System Geometry

CFD simplifications

The geometry used for the CFD simulations was created in order to represent the most relevant aspects of the system. However, due to complex features present in the system, some simplifications were made in order to aid the modeling efforts in terms of numerical stability. These simplifications and main aspects of the geometry will be discussed in this section. Figure 8 shows some elements present in the system.

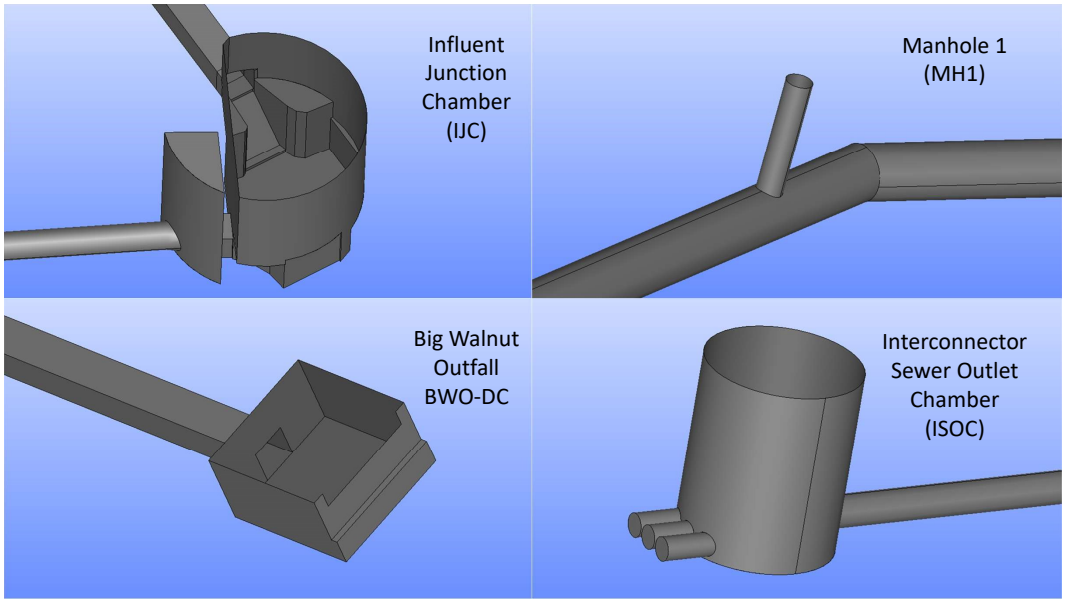

FIG. 8. Important elements represented by the CFD geometry

The key element of this system is the Influent Junction Chamber (IJC). The geometry of this structure was prepared according to drawings and cross sections obtained with ARCADIS. This chamber has 2 sub-chambers, one that receives water only from INT, and the second connected with the inflows from BWO and BWARI, as well with the points where there is the pump outflows. Also, IJC has some geometry features that guides inflows towards the outlet points. Minor simplification such as smoothing the edges and adjusting the total height of IJC were implemented in order to help in the 3-D model's stability.

The representation of INT in the 3-D model starts at the the Interconnect Sewer Outlet Chamber (ISOC), includes the three intermediate, non-ventilated manhole structures,

ending on the IJC. The representation of BWO sewer starts at the BWO-DC chamber that serves as the outfall for IJC, and ends at the IJC. Upstream from BWO-DC, the representation of BWO is made in terms of the head-discharge data that was obtained with the HAST model. Likewise, the representation of BWARI in the 3-D model is also in terms of a head-discharge data from HAST. The ventilation of IJC, INT and related sewers reflected the existing conditions. There is a 24-inch ventilation port to atmosphere at IJC, and no other ventilation points were assumed in the CFD model.

The upstream end of the INT model, the ISOC, had it height increased from 26.04 ft to 46.04 ft given that in the real INT system the sewer continues upstream for miles, and without that there would be an un-physical water overflow. One consequence of this simplification is that the unsteady CFD modeling results following the pump failure are only relevant for the initial seconds (60 seconds). The length of INT represented in the model was 2,200 ft, and at a location 1,845 ft downstream from ISOC there is a change in the direction of INT matching the existing sewer alignment.

4.1.2 Mesh Generation

The mesh was generated used the NETGEN 1D-2D-3D algorithm implemented within SALOME 9.3.0. NETGEN is an automatic 3D tetrahedral mesh generator. The first mesh produced has 323,472 elements. Figure 9 shows the mesh at the IJC as an example and Figure 10 shows the computational cells within slices of the IJC, BWO, INT, and MH1.

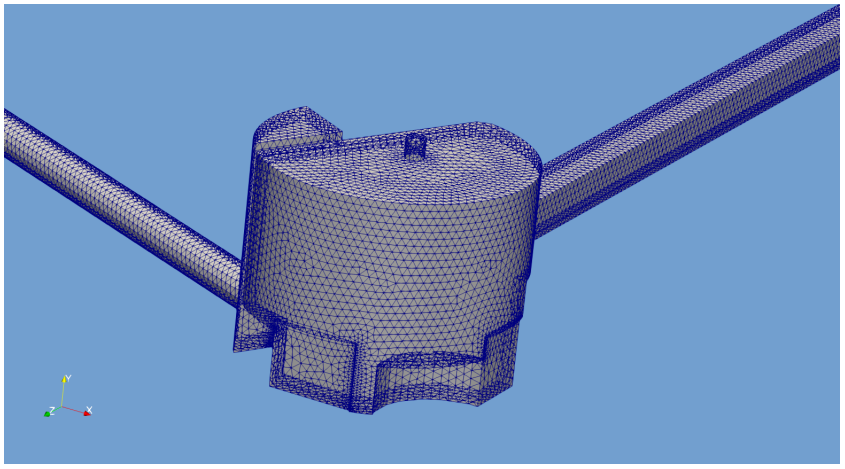

FIG. 9. Mesh at IJC

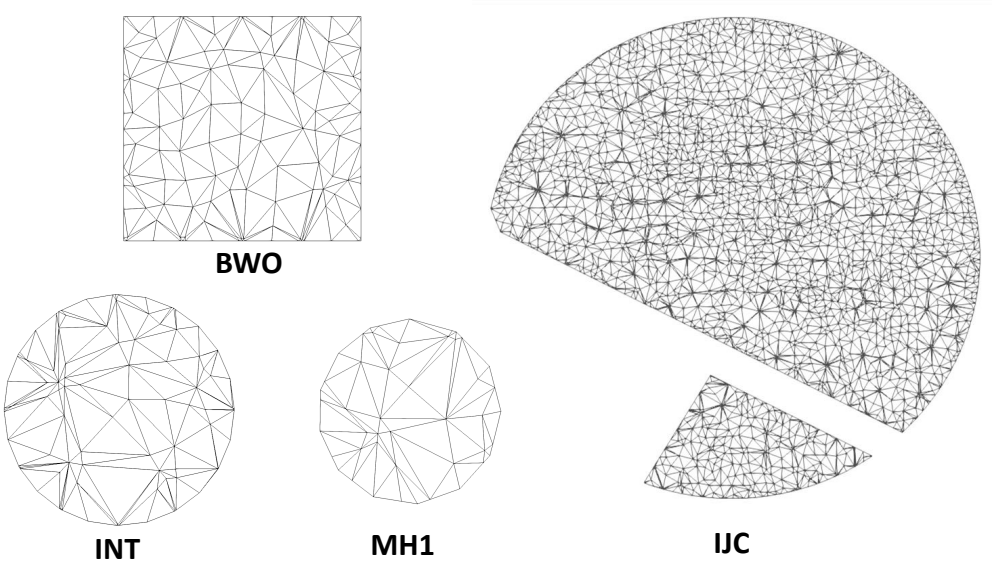

FIG. 10. Computational cells on pipes and chambers cross-sections. Not shown to scale.

A finer mesh was also created in order to verify if this mesh is producing any kind of diffusion that might be impacting the simulations. This finer mesh is shown on Figure 11 and has a total of 949,134 elements. The results of both meshes are alike and there is no diffusion within the simulations. Therefore, the coarser mesh was used due to its faster

computational time and the slices within the sewers were omitted for the sake of brevity.

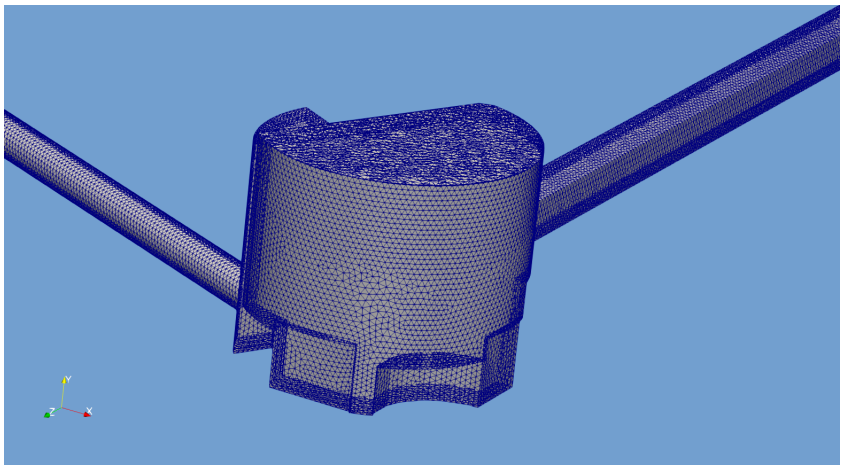

FIG. 11. Finer mesh at IJC

Other meshes were created in order to evaluate modifications within the model. In such cases, the number of computational cells may have a slight difference. However, its does not change significantly from the meshes showed in this section.

4.1.3 OpenFOAM Solver

The first solver used in this work was the *interIsoFoam*. This solver is able to represent two incompressible, isothermal immiscible fluids using isoAdvector phase-fraction based on interface capturing. However, it was found that this solver is not able to represent properly the the air pressurization at MH1. Since this air pressurization is of paramount importance in the simulation, the results obtained by this solver were discarded.

The solver that best represented key processes within the system was the *compressibleInterFoam*. The *compressibleInterFoam* is a solver for two compressible, non-isothermal immiscible fluids using a VOF phase-fraction based interface capturing approach. The next section will discuss its formulation along with the turbulence model selected.

compressibleInterFoam Formulation

In this solver, the water is treated as an incompressible fluid, whereas the air is treated as a perfect gas. A single set of equations for continuity, momentum and energy are solved for the computational domain. The governing equations, continuity (Eq. 1a), momentum equation (Eq. 1b), and energy (Eq. 1c) for a control volume can be expressed, respectively, as (Jadidi et al. 2014; Mohapatra 2016; Olsson 2017):

$$\frac{\partial \rho}{\partial t} + \bigtriangledown.(\rho u) = 0 \tag{1a}$$

$$\frac{\partial (\rho u)}{\partial t} + \bigtriangledown.(\rho u u) = - \bigtriangledown p + \bigtriangledown.(\mu \bigtriangledown u) + S_u \tag{1b}$$

$$\frac{\partial (\rho C_p T)}{\partial t} + \bigtriangledown.(\rho u C_p T) = \bigtriangledown.(k \bigtriangledown T) + S_T \tag{1c}$$

The compressibleInterFoam calculates the physical properties based on phase fraction (α) and carries a value ranging from 0 to 1, where 0 represent the air phase and 1 represents the water phase and the values in-between 0 and 1 represents the interface. The individual fluid properties are calculated as shown in Equations 2a, 2b, and 2c (Jadidi et al. 2014; Mohapatra 2016; Olsson 2017).

$$\rho = \rho_l \alpha + \rho_g (1 - \alpha) \tag{2a}$$

$$\mu = \mu_l \alpha + \mu_g (1 - \alpha) \tag{2b}$$

$$u = u_l \alpha + u_g (1 - \alpha) \tag{2c}$$

where the subscripts $_l$ and $_g$ represent the liquid and gas phase.

The governing equation for the phase transport in this solver uses the two-fluid Eulerian model for two-phase flow. The phase fractions are solved separately for each individual phase, ensuring boundedness and conservativeness of the phase fraction. Equation 3 shows

the transport equation for the compressibleInterFoam (Mohapatra 2016).

$$\frac{\partial \alpha}{\partial t} + \bigtriangledown.(u\alpha) + \bigtriangledown.(u_c\alpha(1-\alpha)) = -\frac{\alpha}{\rho_l}\frac{\mathrm{D}\rho_l}{\mathrm{D}t} \tag{3}$$

Turbulence Modeling

The turbulence model selected for this CFD analysis was the *kOmegaSST*. This model was selected because it combines the *k-omega* turbulence model and *k-epsilon* turbulence model such that the *k-omega* is used in the inner region of the boundary layer and switches to the *k-epsilon* in the free shear flow. The *k-omega* is a common two-equation turbulence model that is used as a closure for the Reynolds-averaged Navier–Stokes equations (RANS equations). The *k-epsilon* turbulence model was conceived to improve the mixing-length model, as well as to find an alternative to algebraically prescribing turbulent length scales in moderate to high complexity flows. Equation 4a shows the equation for the turbulence kinetic energy and Equation 4b shows the specific dissipation rate.

$$\frac{\partial k}{\partial t} + u_j\frac{\partial k}{\partial x_j} = P_k - \beta^* k\omega + \frac{\partial}{\partial x_j}[(\nu + \sigma_k\nu_T)\frac{\partial k}{\partial x_j}] \tag{4a}$$

$$\frac{\partial \omega}{\partial t} + u_j\frac{\partial \omega}{\partial x_j} = \alpha S^2 - \beta\omega^2 + \frac{\partial}{\partial x_j}[(\nu + \sigma_\omega\nu_T)\frac{\partial \omega}{\partial x_j}] + 2(1-F_1)\sigma_{\omega 2}\frac{1}{\omega}\frac{\partial k}{\partial x_i}\frac{\partial \omega}{\partial x_i} \tag{4b}$$

The blending function used to activate the *k-omega* near the wall and the *k-epsilon* in the free stream is shown in Equation 5:

$$F_1 = tanh\left\{\left\{min\left[max\left(\frac{\sqrt{k}}{\beta^*\omega y}, \frac{500\nu}{y^2\omega}\right), \frac{4\sigma_{\omega 2}k}{CD_{k\omega}y^2}\right]\right\}\right\} \tag{5}$$

4.1.4 Initial Conditions

The flow prior to the pump failure is of difficult representation due to many inflows and the system's geometry. There is no initial condition that truly represents the flow.

Therefore, a warm-up is necessary prior to the pump failure. This warm-up was prepared in order to achieve the steady state. 900 seconds were required to achieve the steady state. Then, the pump failure is simulated and different scenarios were tested to evaluate the system's performance.

The initial conditions to start the warm up were set as follow. The water level on the ISOC was set as 25 ft and the water level at the IJC was set as 26.25 ft. The water level at the manholes was set as the pipe diameter in order to let the warm up pressurize the air inside the manholes. The air pressure was set as atmospheric (1e5 Pa) and the velocity was set as 0 ft/s in all directions prior to the warm-up.

4.1.5 Boundary Conditions

This system has multiple inflows, one outflow, and multiple connections to the atmosphere. All of these were treated separately, with specific boundary conditions for a more precise simulation. All the boundary conditions used in the CFD modeling efforts are standard of OpenFOAM and none was created specifically for this analysis.

At ISOC, three pipes were considered discharging a total of 207.5 MGD into the ISOC, each one of them with 69.16 MGD. This inflow propagates into INT, passing through the three manholes with no ventilation and discharging into the IJC.

In this chamber, besides the inflow coming from INT, two other inflows converge into this chamber - Big Walnut Augmentation Rickenbacker Interceptor (BWARI) & Big Walnut Outfall (BWO) - plus the IJC outlet. The BWARI had a fixed inflow of 269.32 MGD until the moment where the pump failed. Then, this value was linearly decreased over 600 seconds to 200.85 MGD. The BWO had an inflow of 141,5 MGD fixed during the simulation. Finally, the IJC outlet had a variable outlet boundary condition, starting with a fixed value of 602.55 MGD, than decreasing for an specific value depending on the selected scenario for 57 seconds, than increasing to 435.94 MGD until the simulation ends.

4.1.6 Cluster & parallelization

Due to the amount of elements required to be calculated in each time-step, the Hopper Cluster located at Auburn, AL, was used. The models were decomposed in small geometries and 30 to 100 processors were used to perform the simulations. Without the cluster and the parallelization, the simulations would not be feasible to be performed.

4.2 Simulation results and discussion

Four scenarios were considered in this analysis. The first scenario considered a very low flow in the IJC outlet after the pump failure. The flow was not set to zero because the standard boundary condition (*flowRateIntetVelocity* (OpenCFD 2019)) cannot handle zero flow. The other three scenarios set the flow after the pump failure as, respectively, 109.55 MGD, 219.11 MGD, and 328.66 MGD. All these scenarios will be discussed in detail on the following sections.

The steady state was achieved at 900 seconds of simulation. At this point, there is no significant velocity or pressure variations within the system. Figure 12 shows the steady state flow in the system. In this figure, it is possible to see that the pressure at the Manhole 1 (MH1) is uniformly distributed throughout its height. Also, the water level at the IJC is greater than at MH1, indicating that the air is compressed in the MH1.

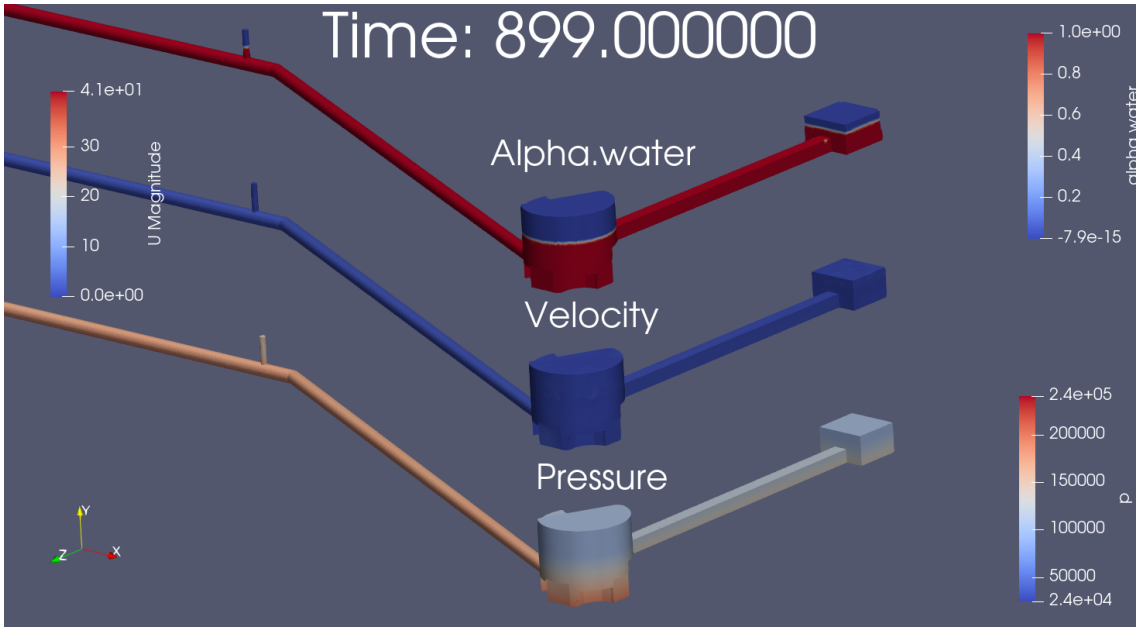

FIG. 12. compressibleInterFoam Steady State

The timeline on the following graphs is based on the pump failure. The starting point (0 seconds) is the moment when the pump fails. At 57 seconds is when the pump restarts. Since the most important phenomena occurs in between these two times, there is no need to extend the results before and after these moments.

4.2.1 Scenario 1: Complete Pump Failure

This first scenario is the most critical since there is no flow and all the water is accumulated on the IJC chamber until it starts to back propagate into the inlet sewers and flow out on the BWO-DC and IJC outlet. Figure 13 shows the water level, velocity and pressure at the moment prior to the pump restarts with a flow rate of 435.94 MGD.

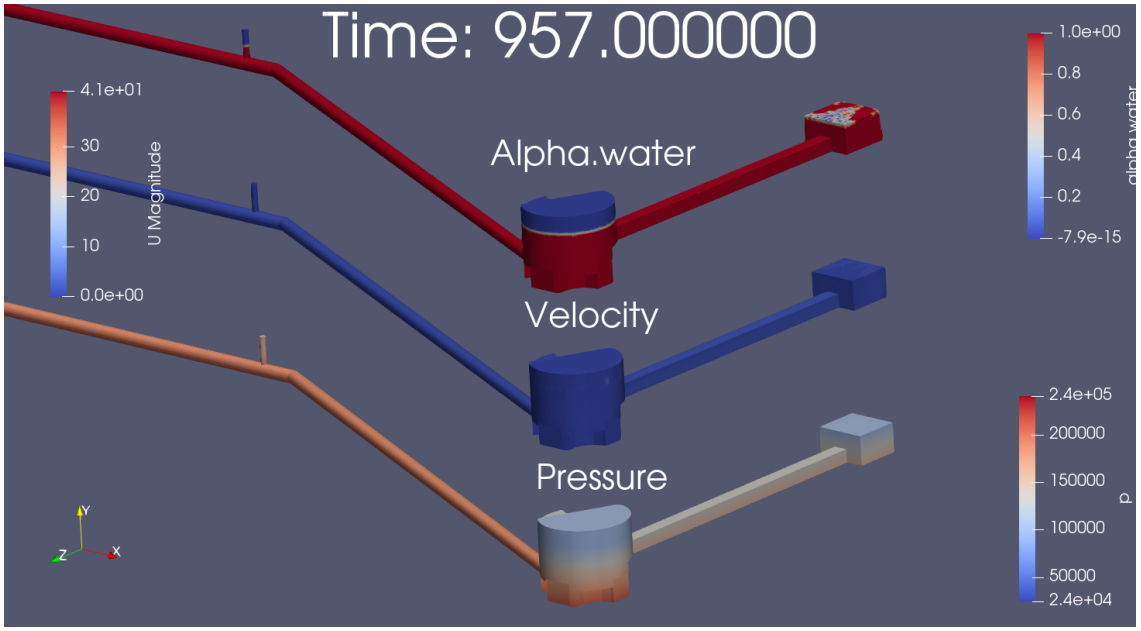

FIG. 13. Scenario 1: Maximum peak level

The CFD simulation results at the IJC chamber along with HAST results for this scenario are shown in Figure 14. In this Figure, it is possible to see that prior to the pump failure the pressure at the bottom of the chamber is 31.03 ft and reaches 36.22 ft at the moment when the pump restarts. This represents a total pressure variation within the chamber of 5.19 ft. HAST predicts a higher pressure variation of 7.30 ft, with a minimum of 30.72 ft and a maximum of 38.02 ft. Since this chamber has a height of 43.5 ft, the water did not flow out through the ventilation.

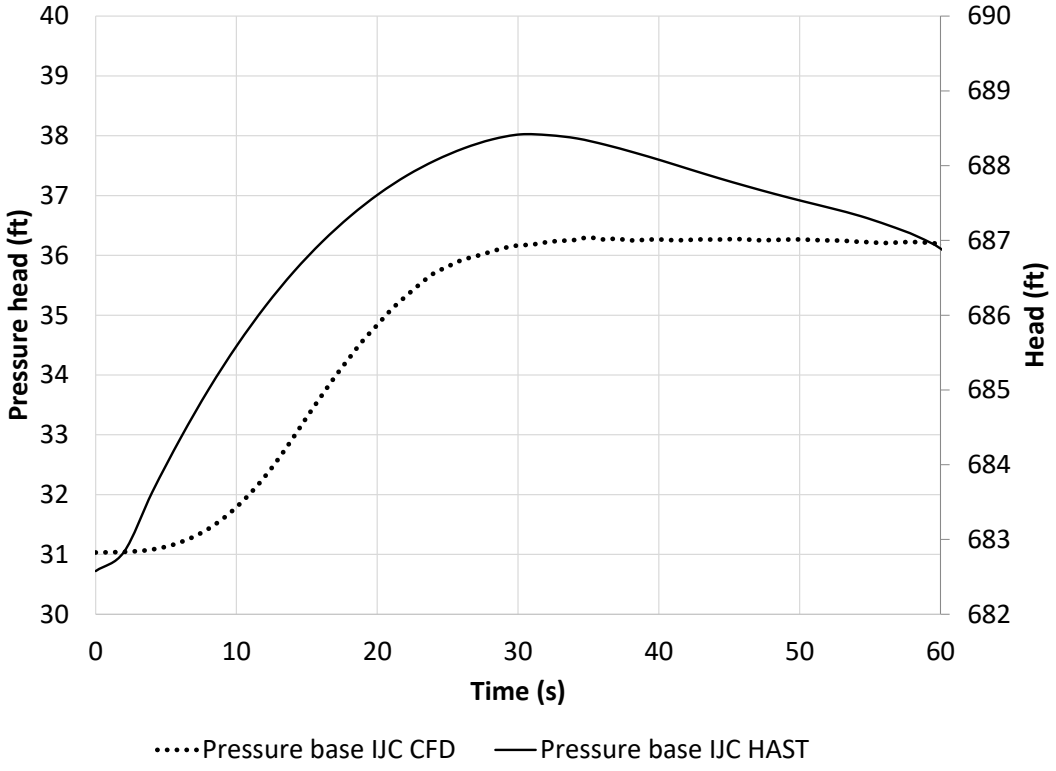

FIG. 14. Scenario 1: Pressure head variation at IJC for CFD scenario 1 along with HAST results

Figure 15 shows the CFD simulation results at the base of the MH1 along with HAST results. Prior the pump failure, at the steady state, the CFD simulation predicts a pressure at the manhole's base of 31.56 ft while HAST predicts a value of 30.45 ft. After the pump failure, the CFD simulation predicts a maximum pressure value of 36.80 ft and HAST predicts a maximum value of 37.33 ft. It is important to highlight that the pressure oscillation is much higher on HAST than on the CFD simulation due to different volumes of air on the initial conditions.

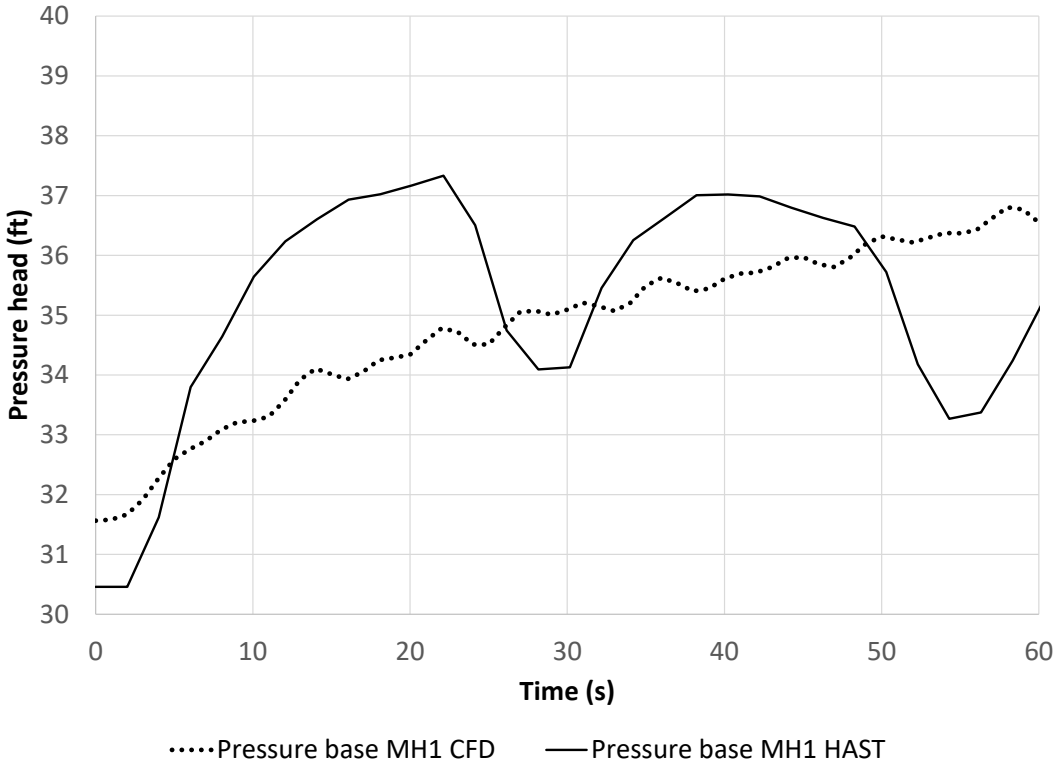

FIG. 15. Scenario 1: Pressure head variation at MH1 for CFD Scenario 1.

4.2.2 Scenario 2: Pump failure to a flow rate of 110 MGD

In this scenario, the pump does not fail completely but keeps rotating with a flow rate of 110 MGD. Figure 16 shows the maximum water level, velocity and pressure prior to the moment that the pump restarts with a flow rate of 436 MGD. At this point, the water is flowing out through the BWO-DC but does not exceed the IJC height.

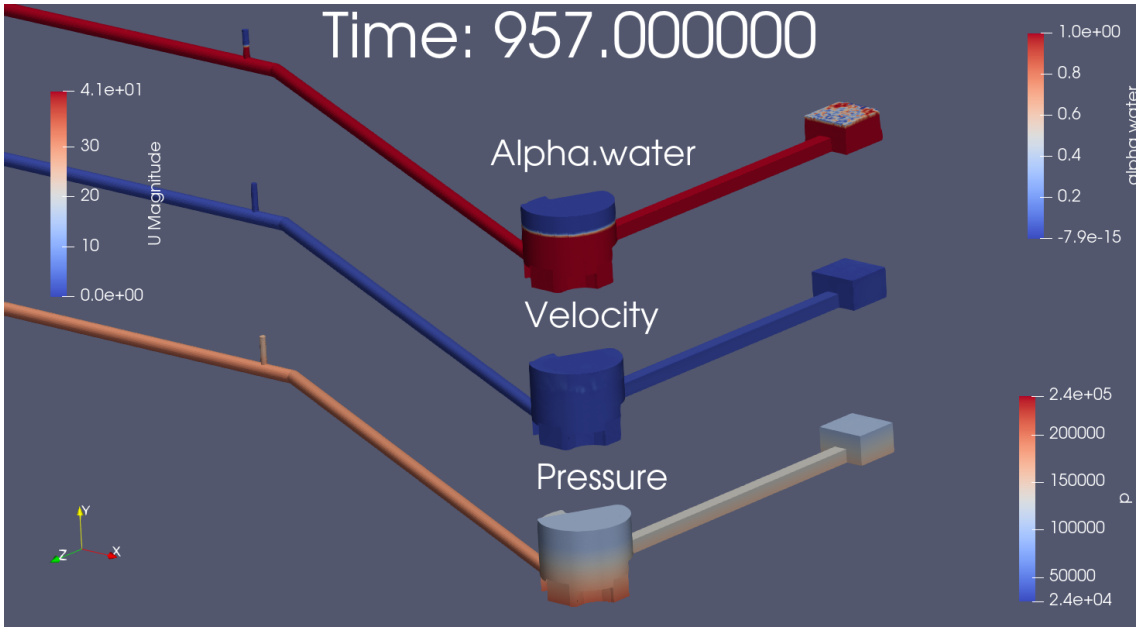

FIG. 16. Scenario 2: Maximum peak level

Figure 17 shows the pressure variation at the bottom of the IJC chamber. In this scenario, the peak pressure prior to the pump restarts is 35.92 ft and, as in scenario 1, it is not greater then the IJC height. A total pressure variation of 4.89 ft within the chamber was predicted by the model considering this scenario.

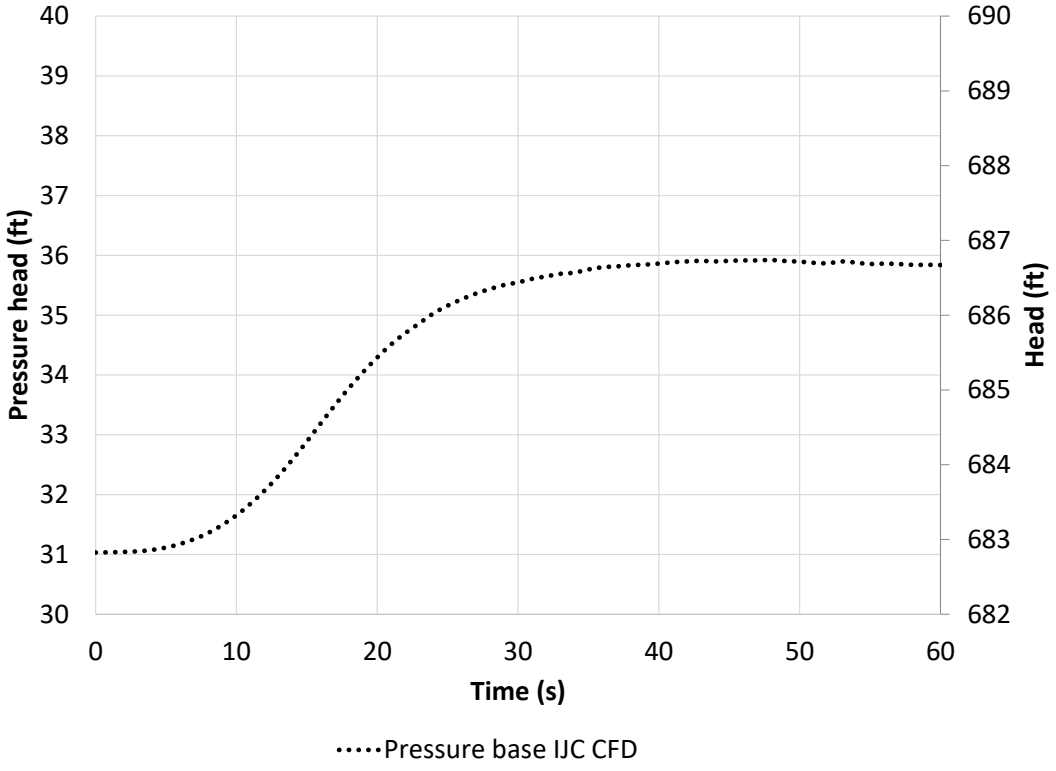

FIG. 17. Scenario 2: Pressure variation at IJC

Figure 18 shows the results at the bottom of MH1 considering this scenario. The maximum pressure at the bottom was 36.04 ft with a total pressure variation of 4.48 ft until the moment of the pump failure.

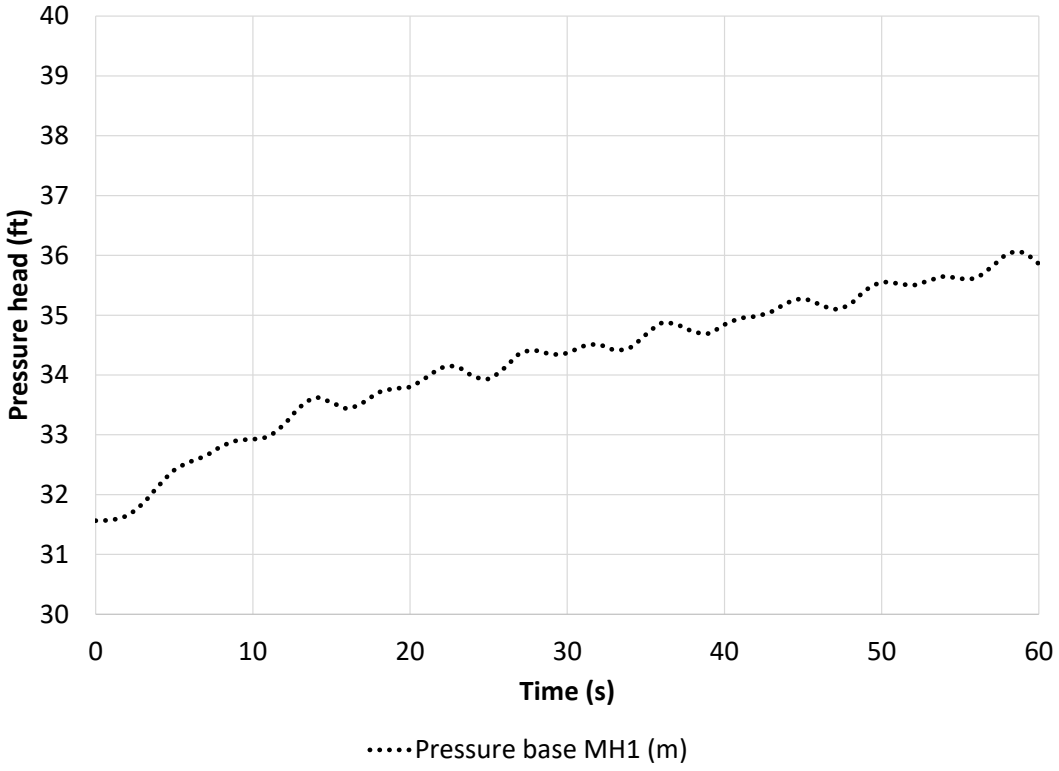

FIG. 18. Scenario 2: Pressure variation at MH1 for CFD scenario 2

4.2.3 Scenario 3: Pump failure to a flow rate of 219 MGD

In this scenario, the pump continues to rotate with a flow rate of 219 MGD. Figure 19 shows the water level, velocity and pressure considering this scenario. It is possible to see some water flowing out at the BWO-DC but, according to the pressure levels obtained in the IJC, no water is flowing out through the IJC ventilation system.

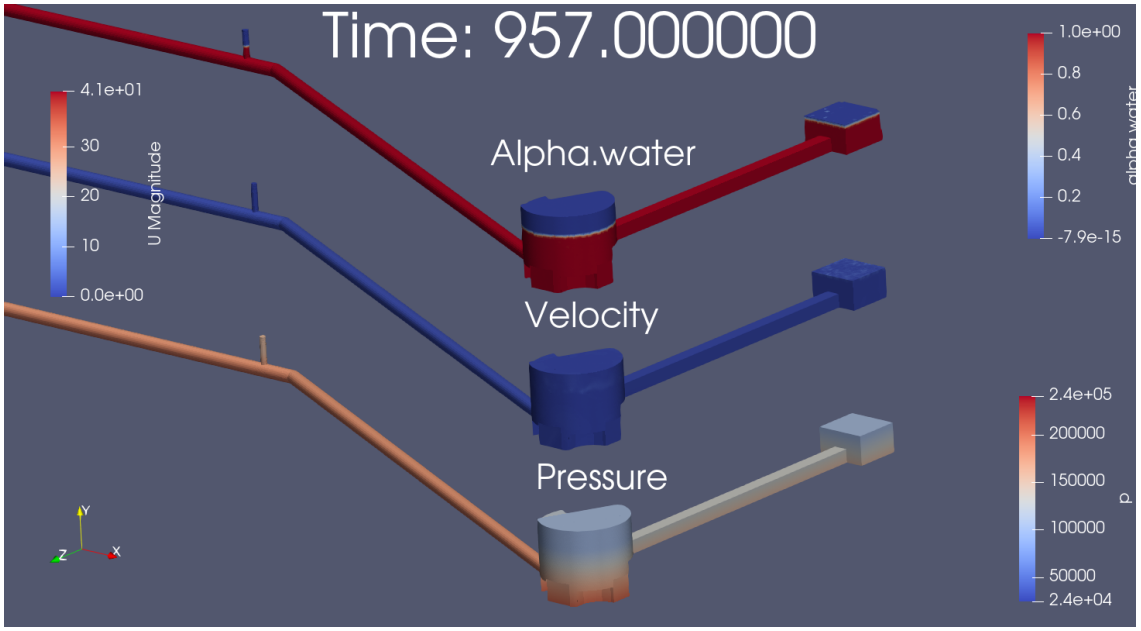

FIG. 19. Scenario 3: Maximum peak level

Figure 20 shows the pressure results at the IJC chamber. In this scenario, the maximum pressure reached at the bottom of the chamber was 35.04 ft, not reaching the IJC maximum height. Therefore, the water is not flowing out of the system through the system's ventilation. The total pressure variation within the IJC considering this scenario is 4.01 ft.

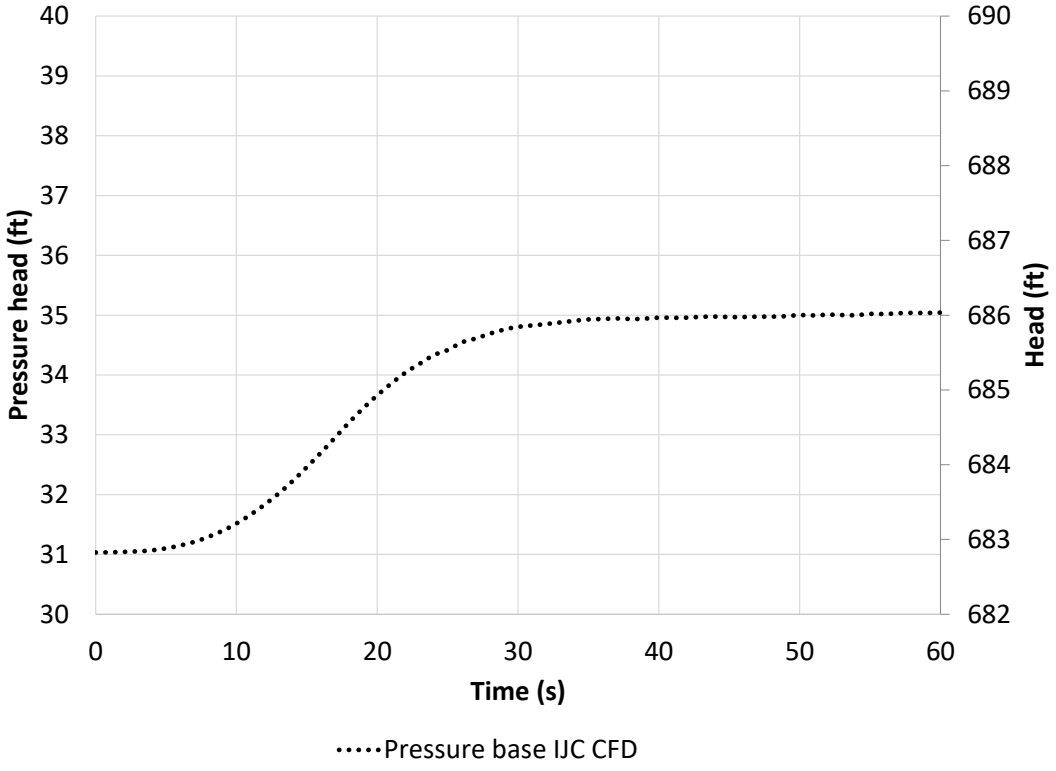

FIG. 20. Scenario 3: Pressure head variation at IJC for CFD scenario 3

Figure 21 shows the results at MH1 for this scenario. The bottom of the manhole reached a maximum pressure of 35.20 ft. The pressure difference was 3.64 ft.

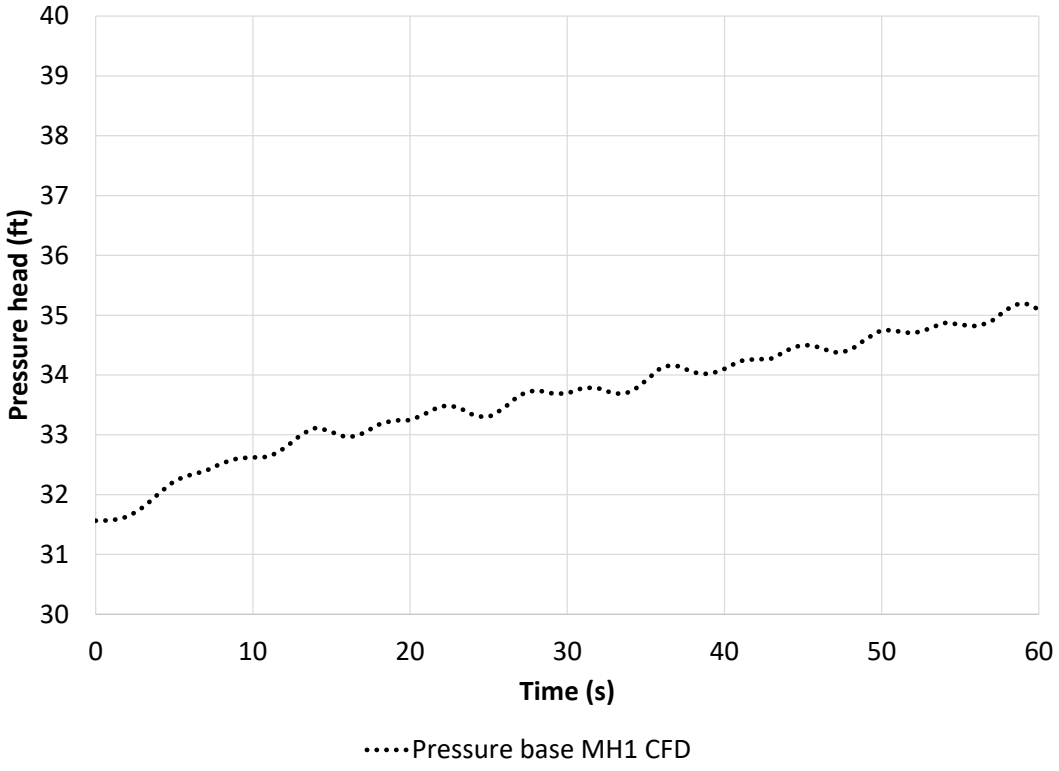

FIG. 21. Scenario 3: Pressure head variation at MH1 for CFD scenario 3

4.2.4 Scenario 4: Pump Failure 329 MGD

The last scenario considered in this analysis had a flow rate of 329 MG after the pump stopped working. This can be considered the less critical scenario analyzed in this work. Figure 22 shows the water level, velocity, and pressure at the moment prior to the pump restarts. Some water is leaving the system through the BWO-DC, but the amount is not as significant as the previous scenarios.

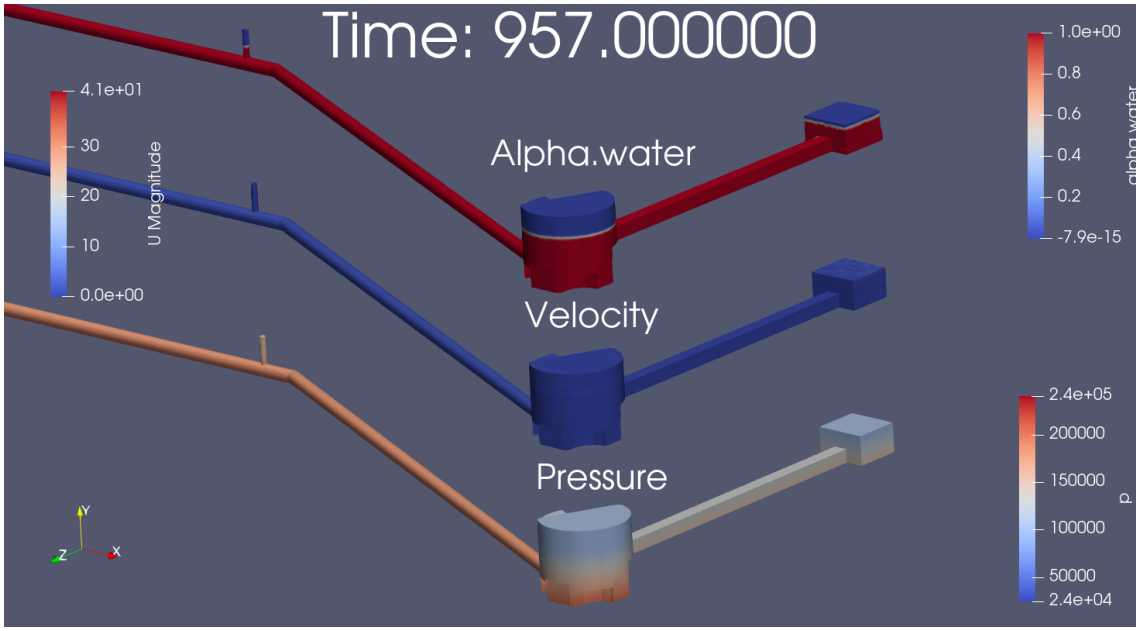

FIG. 22. Scenario 4: Maximum peak level

Figure 23 shows the pressure variation on the IJC chamber for this scenario. It achieved a maximum of 34.18 ft after the pump failure. This value is less than the IJC height and, therefore, no flow out through the system's ventilation. The pressure difference was only 3.15 ft.

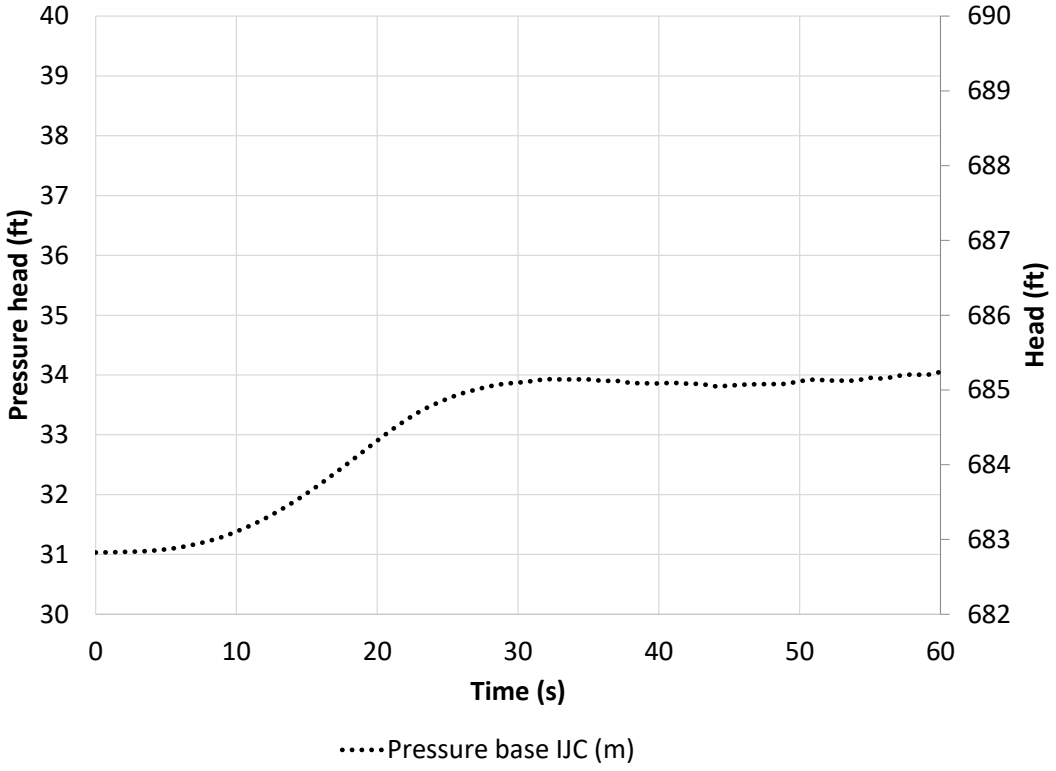

FIG. 23. Scenario 4: Pressure head variation at IJC for CFD scenario 4

Finally, Figure 24 shows the results for the bottom of the manhole. The bottom of the manhole reached a maximum pressure of 34.26 ft right before the pump restarts. The pressure difference was 2.7 ft for the bottom of the manhole.

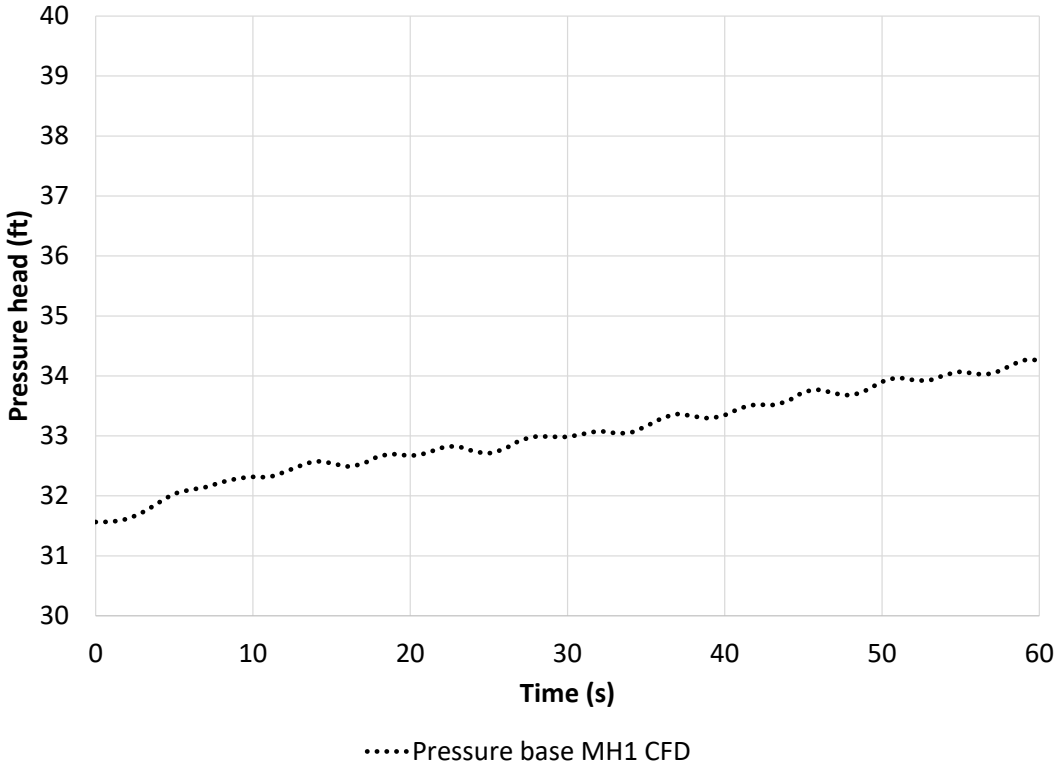

FIG. 24. Scenario 4: Pressure head variation at MH1 for CFD scenario 4

4.2.5 Summary of all CFD Simulation

The CFD results indicate, as expected, that the most critical scenarios (1 & 2) linked with more severe pump disruption led to the conditions with the highest pressure variation at the IJC and MH1. Yet, compared with the results obtained with HAST, the results for the pressure rise at the base of MH1 obtained with the CFD model was not as high as the results yielded by HAST. There could be various causes for the discrepancy between the models, which could include the difference in the mathematical models and the more simplified system geometry representation used in the CFD model.

Figure 25 summarizes the differences between the scenarios on the IJC and Figure

26 shows the difference between the scenarios on the MH1.

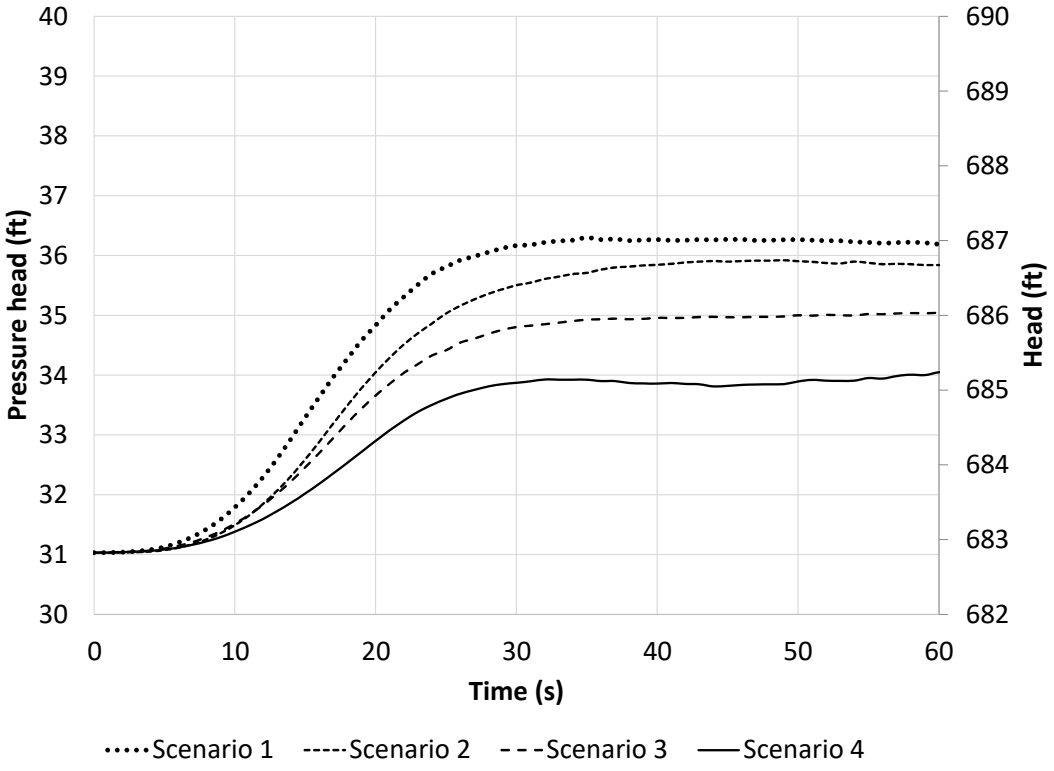

FIG. 25. CFD simulation results considering all scenarios for IJC

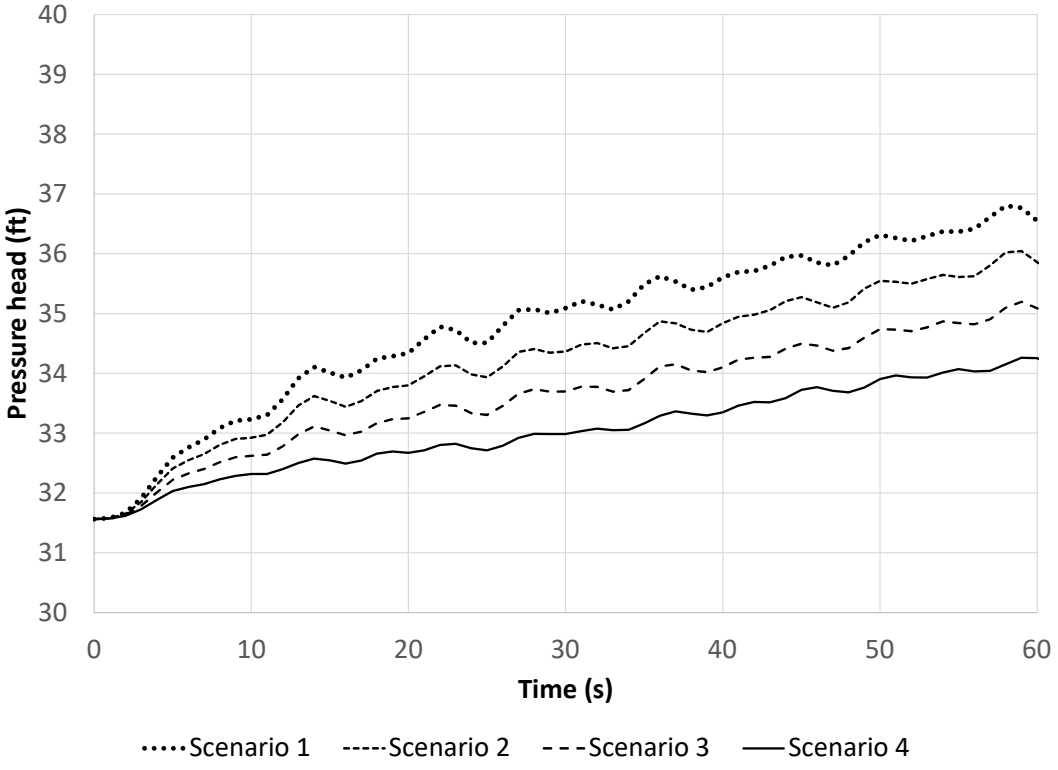

FIG. 26. CFD simulation results considering all scenarios for MH1

These results indicated that the 1D simulation results are more conservative while being consistent with CFD results. Part 3 of the report will perform 1D simulation of an alternative for INT that includes two-barrels at the end of the INT while ventilating MH1.

5 Part 3: Alternative INT design with ventilated MH1

An alternative for countering the effects of the air pressurization at MH1 that have led to the displacement of the concrete structure at the top would be to allow for the ventilation of air. With that, the buoyancy force and the dynamic air phase pressure force would be removed. On the other hand, an upward water phase pressure force underneath the structure would appear, but as it will be shown below the resulting forces are still downward and show that the structure would remain stable even in an eventual repetition of the complete pump failure with river flooding from March 19 and 20, 2020.

5.1 Simulation conditions

This Part presents the results from the HAST3 modeling for the entire INT, BWO, BWARI and IJC system, considering that the terminal reach of INT has already a twin-barrel geometry after the Sewer Outlet Chamber. The inflows were the same as the conditions presented in Part 1, and the water level is impacted by the flooding of the Scioto River, at an stage elevation of 684 ft.

Aside from the twin-barreled configuration of the the INT, the second modification that was introduced to the model was the presence of a 12-in ventilation tower that is placed at the top slab of the concrete structure. The ventilation tower has a top elevation of 692.3 ft, where there is contact with atmospheric air.

5.2 Simulation results

Simulation results performed with these conditions indicate that the pressures at IJC and MH1 follow the same overall pattern, with a higher frequency of oscillation at MH1 created by the smaller plan area of MH1. This is indicated with the pressure head results from the two locations presented in Figure 27.

FIG. 27. Comparison of head elevation between IJC and MH1 for a scenario where there is a 12-in ventilation tower at MH1.

In the absence of air, the force balance in MH1 is changed as there will be no air phase pressure force nor the buoyant force created by the air presence. On the other hand, an upward water pressure force acting underneath the concrete structure appeared in the solution. This pressure acts at the elevation 677.6 ft, and correspond to a hydrostatic elevation of 690 ft, which is the maximum water level calculated in the simulations for the MH1 ventilation tower. As a result, the following are the forces acting on the vented scenarion for MH1:

1. Concrete structure weight, 140 ft^3 of volume, weight of 9.9 ton-force, downward
2. Hydrostatic pressure force acting on the top of structure, 7'8" diameter, depth of 5.5 ft, 7.2 ton-force, downward
3. Hydrostatic pressure force acting on the 1'8" wide outer concrete ring with center line diameter of 6 ft, positioned 4 ft below the top slab, equal to 8.5 ton-force, upward.
4. Dynamically varying water pressure force underneath MH1 slab, with a maximum value of 5.2 tons-force.

Force components from 1 to 4 result in a minimum downward resulting force of 3.3 ton-force. Thus, even when the water level reaches the maximum at the ventilation tower the forces will not displace the concrete structure at the top of MH1.

6 Final remarks

In this report, the performance of the INT, BWO and BWARI sewers were evaluated numerically through scenarios that involved failure (complete and partial) of the pumps placed on the IJC at the entrance of the Southerly WWTP in Columbus, OH. This evaluation was made in terms of using a 1D hydraulic model, HAST, and a 3D Computational Fluid Dynamics (CFD) tool, OpenFOAM. The 1D model intended to capture the system-wide unsteadiness of the sewers through the period from 12 AM in March 20, 2020, including the pump failure. The 3D model was used to represent just the instants prior to and after the pump failure, with focus only on the structures IJC and MH1.

This report has indicated that the forces associated with the air pressurization in the headspace of MH1 could have create conditions that would explain the structural damage observed on that site. The balance of forces acting on the top concrete structure exceeded the downward stabilizing forces during the rain event. A significant portion of these forces were created by the dynamic air phase pressure change that resulted from the pump failure at IJC and subsequent rise of the WL, and pressure, in IJC and the nearby structures.

CFD results explored the flow characteristics with much detail near IJC and MH1 following a complete pump failure. However, the 3D study also included potential differences between a complete pump failure and other alternative scenarios where the failure was not complete. It demonstrated that the complete pump failure created a faster rate of change in IJC, as expected. The results from CFD and from the HAST model were compared, and while they are not exactly the same these are consistent and comparable. One positive outcome from the CFD study was that there was no significant air entrainment occuring by the inflows arriving at IJC that would have contributed to the problems observed in MH1.

The final part of the report explored an alternative geometry for the system using HAST model, with a twin-barreled terminus for the INT sewer and a 12-in ventilation

tower installed at MH1. While the pressures measured at the bottom of MH1 were not significantly changed with the ventilation, the elimination of the air phase at the headspace of MH1 altered the force balance and reduced the upward forces acting on MH1 in an failure scenario that was equivalent to the one observed in March 20, 2020. The results from the simulation indicate that there would be no conditions for a similar failure to occur after the ventilation was installed.

References

Jadidi, M., Tembely, M., Moghtadernejad, S., and Dolatabadi, A. (2014). "A coupled level set and volume of fluid method with application to compressible two-phase flow." *Proceedings of the 22nd Annual Conference of the CFD Society of Canada, Toronto, ON, Canada*, 1–4.

Mohapatra, C. (2016). "Computational study of internal two phase flow in effervescent atomizer in annular flow regime." M.S. thesis, University of Cincinnati, 2600 Clifton Ave, Cincinnati, OH 45221.

Olsson, E. (2017). "A description of isoadvector-a numerical method for improved surface sharpness in two-phase flows." *Proceedings of CFD with OpenSource Software, Edited by Nilsson. H.*

OpenCFD (2019). *OpenFOAM - The Open Source CFD Toolbox - User's Guide*. OpenCFD Ltd., United Kingdom, 7 edition (11April).

Vasconcelos, J. G., Klaver, P. R., and Lautenbach, D. J. (2015). "Flow regime transition simulation incorporating entrapped air pocket effects." *Urban Water Journal*, 12(6), 488–501.

Vasconcelos, J. G., Wright, S. J., and Roe, P. L. (2006). "Improved simulation of flow regime transition in sewers: Two-component pressure approach." *Journal of hydraulic engineering*, 132(6), 553–562.